Mapping Hydrogen Positions along the Proton Transfer Pathway in an Organic Crystal by Computational X-ray Spectra†

Guoyan Ge,[a] Jun-Rong Zhang,[a] Sheng-Yu Wang,[a] Minrui Wei,[a] Yongfei Ji,[b] Sai Duan,[c] Kiyoshi Ueda,[de] and Weijie Hua*[a]

Understanding the proton transfer dynamics through hydrogen bonds is a fundamental issue in chemistry, especially in condensed phases. While time-resolved X-ray spectroscopy offers a unique probe localized within the hydrogen bonds, accurate interpretation remains a challenge and relies on high-quality theoretical spectral references that map the proton motions. Here, with hybrid quantum mechanical and molecular mechanical (QM/MM) simulations, we computed a two-dimensional (2D) map of the N1s X-ray photoelectron/absorption spectra (XPS/XAS) for an organic crystal, composed of protonated 4,4'-bipyridine ($BpyH^+$, acceptor) and 5-sulfosalicylic acid ($Sulfo^-$, donor), with respect to varying hydrogen positions at nitrogens N1 and N2 of $BpyH^+$. We obtained a continuous picture of each spectrum and the chemical shift, mapping the proton transfer processes from O–H···N to $O^-\cdots H^+$–N at N1 and from $O^-\cdots H^+$–N to O–H···N at N2. We demonstrate that N1s transient XPS/XAS spectra are sensitive probes for hydrogen positions and proton transfer processes. We observe that reducing the O–H distance at the N1 site by only 0.2 Å, compared to the crystal structure determined from X-ray diffraction (XRD), provides an excellent match between the QM/MM and experimental spectra, consistently in both XPS and XAS. Our calculations also demonstrate that geometry optimizations with periodic boundary conditions are difficult to refine the proton positions in experimental crystal structures, whereas our scaled snapshot protocol offers a more effective way. Our study reveals a nonlinear behavior of the absorption energy for the π_1^*/π_2^* peak in XAS with increasing N–H distance, exhibiting a distinct barrier at around 0.95 Å. This study provides a clear mapping of the two correlated proton transfer dynamics into X-ray spectra within a complex crystal, offering insights for future transient experimental studies.

Introduction

Understanding the ultrafast dynamics of proton transfer (PT) is a fundamental challenge in chemistry, given its crucial role in numerous chemical and biological processes, such as acid-base neutralization, fuel cell operation, and enzymatic reactions.[1–5] PT can occur in gas, liquid, and crystal phases, and both in the ground electronic states and excited states (known as excited-state intramolecular PT, ESIPT). Generally, understanding PT in condensed phases (liquid and solid) is more challenging than in the gas phase, owing to increased intermolecular interactions, solvent effects, structural constraints, and kinetic factors. In the liquid phase, differences in pK_a values among residues can affect PT, with increased acidity or basicity often initiating these processes.[1–5] In organic crystals with intra- or inter-molecular hydrogen bonds (HBs), PT can be triggered by thermal or photo stimuli and occur along the HBs.[6,7] The potential energy surfaces (PESs) along the PT coordinate determine the possibility and rate of the reaction, influenced by various factors such as hydrogen bonding, Coulomb interactions, charge transfer interactions, van der Waals interactions, and ambient conditions.[8] Recent studies have used femtosecond spectroscopy to investigate the ultrafast dynamics of PT and shed light on the interplay between electronic

[a] MIIT Key Laboratory of Semiconductor Microstructure and Quantum Sensing, Department of Applied Physics, School of Physics, Nanjing University of Science and Technology, 210094 Nanjing, P. R. China E-mail: wjhua@njust.edu.cn
[b] School of Chemistry and Chemical Engineering, Guangzhou University, Guangzhou, Guangdong 510006, P. R. China
[c] Collaborative Innovation Center of Chemistry for Energy Materials, Shanghai Key Laboratory of Molecular Catalysis and Innovative Materials, MOE Key Laboratory of Computational Physical Sciences, Department of Chemistry, Fudan University, Shanghai 200433, P. R. China
[d] School Physical Science and Technology, ShanghaiTech University, Shanghai 201210, P. R. China
[e] Department of Chemistry, Tohoku University, Sendai 980-8578, Japan

† Electronic Supplementary Information (ESI) available: Computational details; Validation of point charge types; Validation of the effect of point charges; Parameters for atomic charges; Parameters for HB structures; Figures for QM/MM models; Figures for model variants in the terminals and spectra; Figure for ground- and core-state PECs. See DOI: XXX/XXXXX/

and nuclear degrees of freedom.[?,?,?]

In the context of studying the 3D structure of atoms in crystals, X-ray diffraction (XRD) is a widely used technique. However, accurately determining the positions of hydrogen atoms poses a significant challenge due to their extremely low scattering cross-sections.[?] Additionally, the fast classical motions of hydrogen atoms and the spread of their quantum wavepacket further complicate the determination. Time-resolved X-ray or electron scattering techniques can capture structural dynamics in real time, but the spatial resolution is relatively low. Although neutron diffraction[?] is considered the gold standard for determining the positions of hydrogen atoms, it requires larger sample amounts and is limited by the availability of neutron sources. Time-resolved neutron scattering with a temporal resolution of ~ns is suitable for probing kinetics but not wavepacket dynamics.

On the other hand, X-ray spectroscopy offers exceptional local sensitivity, despite not providing 3D information. The locality of inner-shell electron excitations allows analyses of chemical shifts, atomic populations of valence orbitals, and distances within the vicinity. Consequently, X-ray spectroscopy is highly sensitive to processes such as proton transfer occurring in close proximity to the probed atom. It has been widely utilized to determine protonation states in various contexts, including gas-phase molecules,[?,?] solutions,[?] and organic crystals.[?,?,?] X-ray photoelectron (XPS)[?,?,?,?,?,?] and absorption (XAS)[?,?,?] spectra are the two most common techniques for organic crystals, providing detailed information on proton dynamics associated with hydrogen bonding.

Time-resolved X-ray spectroscopy provides a more direct approach to investigate chemical reactions.[?,?,?,?] The development of X-ray free electron lasers (XFEL)[?,?,?] and high harmonic generation (HHG)[?,?,?,?,?,?] sources has advanced the capabilities of probing. Transient X-ray absorption spectroscopy (TXAS) [also often termed time-resolved XAS (tr-XAS) or X-ray transient absorption spectroscopy (XTAS)], is a powerful tool for capturing electronic and nuclear dynamics.[?,?,?] Garratt et al.[?] utilized TXAS at the carbon K-edge to study the ultrafast exciton localization dynamics of the P3HT polymer. They combined experimental measurements with time-dependent density functional theory (TDDFT) calculations to interpret the spectral signatures. Pertot and co-workers[?] employed femtosecond TXAS at the carbon K-edge and sulfur L-edges to characterize the photoinduced dissociation pathways of gas-phase CF_4^+ and SF_6^+ cations, using both experimental and computational approaches. Leone and co-workers[?] investigated the ultrafast intersystem crossing dynamics of the enolic form of acetylacetone using femtosecond TXAS at the carbon K-edge, in conjunction with TDDFT calculations. Leone et al.[?] also utilized femtosecond TXAS to study the ultrafast evolution of valence electronic structure in the electrocyclic ring-opening process of 1,3-cyclohexadiene, complemented by TDDFT simulations. Wolf et al.[?] demonstrated that TXAS is sensitive to the ultrafast electronic relaxation of $\pi\pi^*/n\pi^*$ excited-state internal conversion using thymine as a model system, supported by high-level coupled cluster calculations. On the other hand, transient XPS (TXPS), also known as time-resolved XPS (tr-XPS), provides valuable information on the local charge and bonding properties of specific atoms. It has been extensively used to investigate various photoinduced dynamics, including charge distribution of molecules,[?] interfacial charge transfer,[?,?] and dissociation.[?,?,?]

In this work, we focus on the proton position along the PT pathway in a complex organic crystal called 4,4'-bipyridine/5-sulfosalicylic salt crystal[?] (BSC, see Figure 1a). This crystal is synthesized by 4,4'-bipyridine (Bpy) and 5-sulfosalicylic acid (Sulfo). Structurally, it is composed of the protonated Bpy ($BpyH^+$) acceptor and the $Sulfo^-$ donor (Figure 1b), with nitrogen atoms only appearing in the $BpyH^+$ acceptor. At each of the two nitrogens N1 and N2 in $BpyH^+$, an HB is formed with the neighboring $Sulfo^-$ residue in the crystal. The unprotonated nitrogen N1 forms a strong N···H–O type HB with a distance of $r_{NO} = 2.5$ Å, while the protonated nitrogen N2 forms a normal $N–H^+\cdots O^-$ type HB with a distance of $r_{NO} = 2.7$ Å. N1s ionization/excitation thus provides a direct probe to the PT dynamics at N1 and N2. We will use the protocol of snapshots along the PES[?,?] to simulate the TXPS and TXAS spectra along the PT path, and to investigate the relationship between the proton transfer dynamics and X-ray spectra in such complex organic crystals. Within this framework, one obtains for instance, the TXAS signal $S_{\mathrm{TXAS}}(\omega,\zeta)$ in terms of the *reaction coordinate* ζ, instead of the signal $S_{\mathrm{TXAS}}(\omega,\tau)$ in terms of the time delay τ (ω denotes the photon energy).[?] At each snapshot, we map out the core ionization or excitation from the ground electronic state, providing computed maps of XPS or XAS that correspond to the proposed infrared (IR)-pump–X-ray-probe[?,?] and the terahertz (THz)-pump–X-ray-probe[?,?] spectroscopies.

Results

XPS at the crystal structure

To simulate the X-ray spectra of the BSC crystal, four QM/MM models 1-4 with increasing sizes (Figures 1 a-c and S1) were constructed at the crystal structure[?] based on a 3 × 3 × 3 supercell. The QM part consisted of neighboring residues to a $BpyH^+$ residue in the center of the supercell (termed as the central residue[?]), while the rest atoms were classified as the MM part. DFT with the BP86 functional[?,?] was used for the QM part, and point charges obtained by using the natural population analysis (NPA)[?] were employed for the MM part. Figure 1 d-f illustrates the simulated N1s XPS and XAS spectra of BSC at its crystal structure with models 1-4. In Figure 1d, the experimental XPS spectrum[?] exhibits two peaks at 399.40 and 401.33 eV (Δ=1.9 eV) with almost identical intensities. They correspond to the (unprotonated) pyridinic (=N–) nitrogen N1 and the protonated pyridinic (=NH^+–) nitrogen N2, respectively (Figure 1b). Theoretical spectra show rapid convergence in both energy and profile as the cluster size increases. Each theoretical spectrum has been adjusted to coincide with the experiment by aligning the N2 peak. The relative binding energies between N1 and N2 are 1.6, 1.6, and 1.5 eV for models 2, 3, and 4, respectively. The difference between the two largest models is approximately 0.1 eV, and the deviation of the largest model 4 from the experiment (1.9 eV) is 0.4 eV. Additional calculations with larger models, including more stacking residues, were also performed but did not

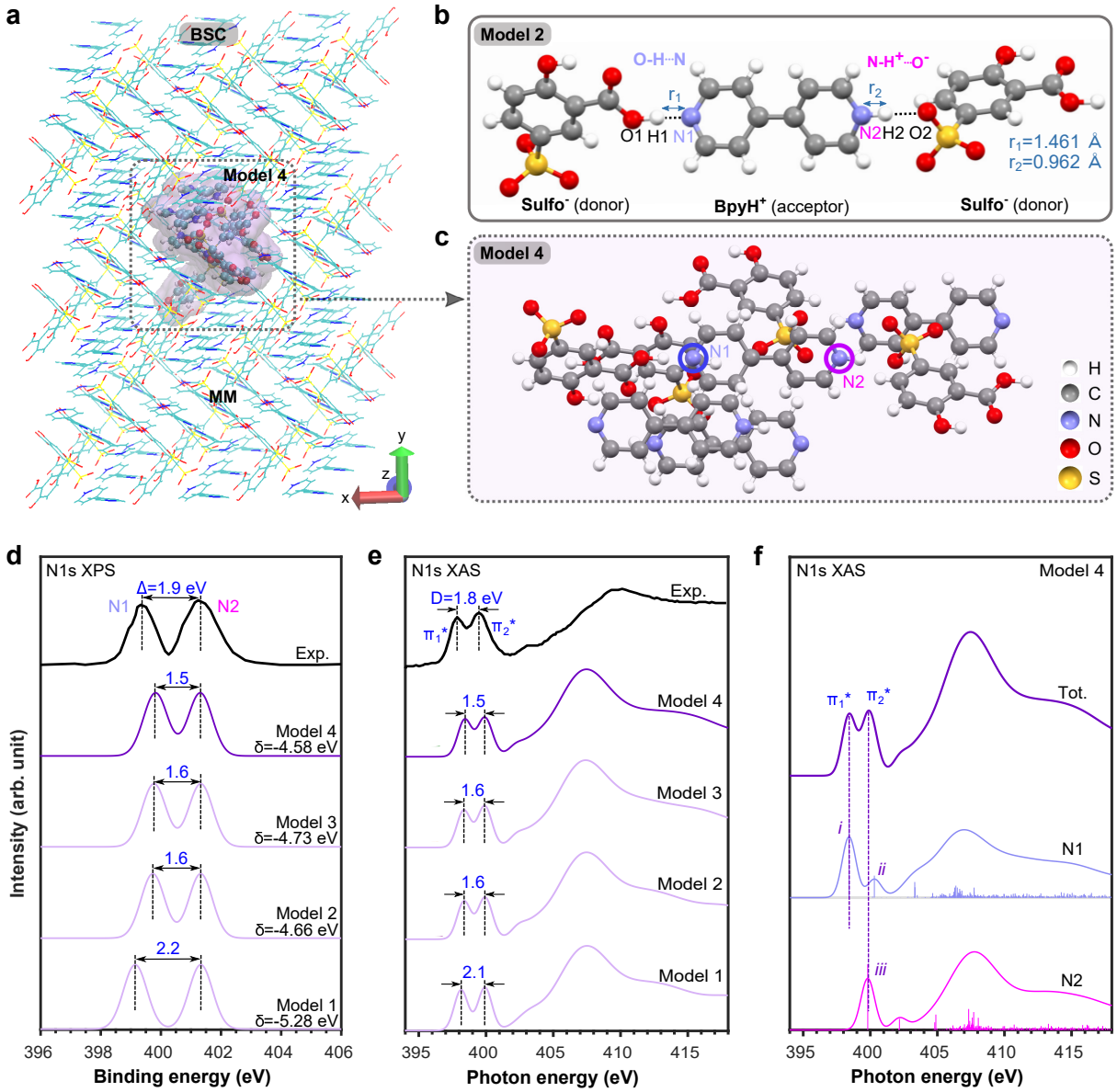

Fig. 1 (a-c) Structure of the BSC crystal and (d-f) X-ray spectra computed at the crystal structure. (a) Constructed QM/MM model 4 based on a 3×3×3 supercell. The model has the largest QM part compared to other models (models 1-3). (b-c) The QM parts of models (b) 2 and (c) 4 constructed by including surrounding residues to the central $BpyH^+$ residue (acceptor). (See structures of models 1 and 3 in Figure S1). In panel b, one O-H···N and one $O^-\cdots H^+$-N hydrogen bonds are formed at nitrogens N1 (unprotonated) and N2 (protonated) of $BpyH^+$, respectively, with the two nearest $Sulfo^-$ donors. N–H distances at the XRD crystal structure are given in Å. (d-e) Simulated total N1s (d) XPS and (e) XAS spectra of BSC with different QM/MM models. (f) Analysis of atomic-specific contributions to the total XAS spectrum simulated with model 4. Major peaks are labeled. Theoretical XPS have been shifted by δ to better compare with the experiment[?] by aligning the high-energy peak; no *ad hoc* shift was applied in XAS.

change the result. It is necessary to note that even for gas phase molecules, ΔKohn-Sham (ΔKS)[???] based calculations introduce a deviation of around 0.5–1 eV[???]. Similar accuracy has been observed in other organic crystals[?].

XAS at the crystal structure

In Figure 1e, the XAS spectra also show rapid spectral convergence with the model size, similar to XPS. Stevens et al.[?] identified two π^* peaks, π_1^* (397.7 eV) and π_2^* (399.5 eV), separated by D=1.8 eV. Our calculation based on model 4 positioned the two peaks at 398.4 and 399.9 eV, respectively, with D=1.5 eV. The deviation from the experiment is approximately 0.3 eV. Concerning the intensities, our simulation using model 4 yielded a satisfactory profile that aligns with the experiment.[?] In Figure 1f, the atomic-specific XAS spectra (using model 4) provide additional insights. It is observed that π_1^* is mainly attributed to N1 (indicated as peak i), while π_2^* is predominantly contributed by N2 (peak iii), with a relatively minor contribution from N1 (peak ii).

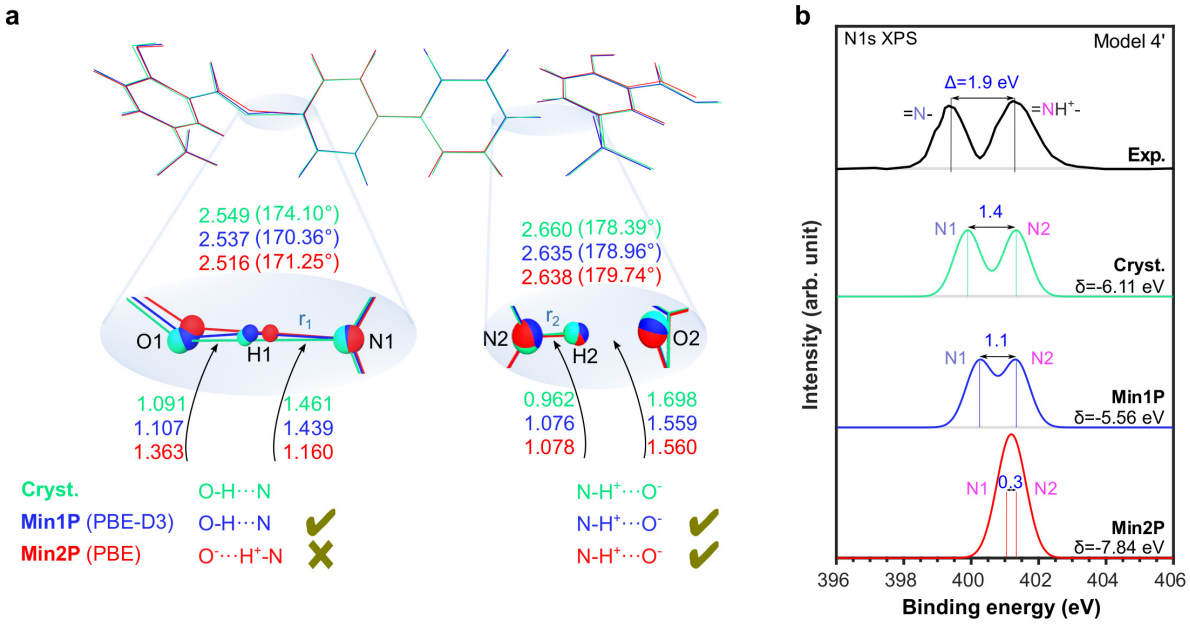

Fig. 2 (a) Superposition of two PBC-optimized structures of BSC by using PBE-D3 (**Min1P**, blue) and PBE (**Min2P**, red) functionals, together with the XRD crystal structure[?] (**Cryst.**, green). Two functionals yielded different predictions regarding the types of hydrogen bonds at N1, which align with the crystal structure (indicated by a checkmark) or not (cross mark). Both functionals agreed on the type of HB present at N2, which matches the crystal structure. Bond lengths (O-N, O-H, and N-H) in Å and angles (∠OHN) in ° are labeled. (b) Simulated N1s XPS spectra at the three geometries. Theoretical XPS have been shifted by δ to better compare with the experiment[?] by aligning the high-energy peaks.

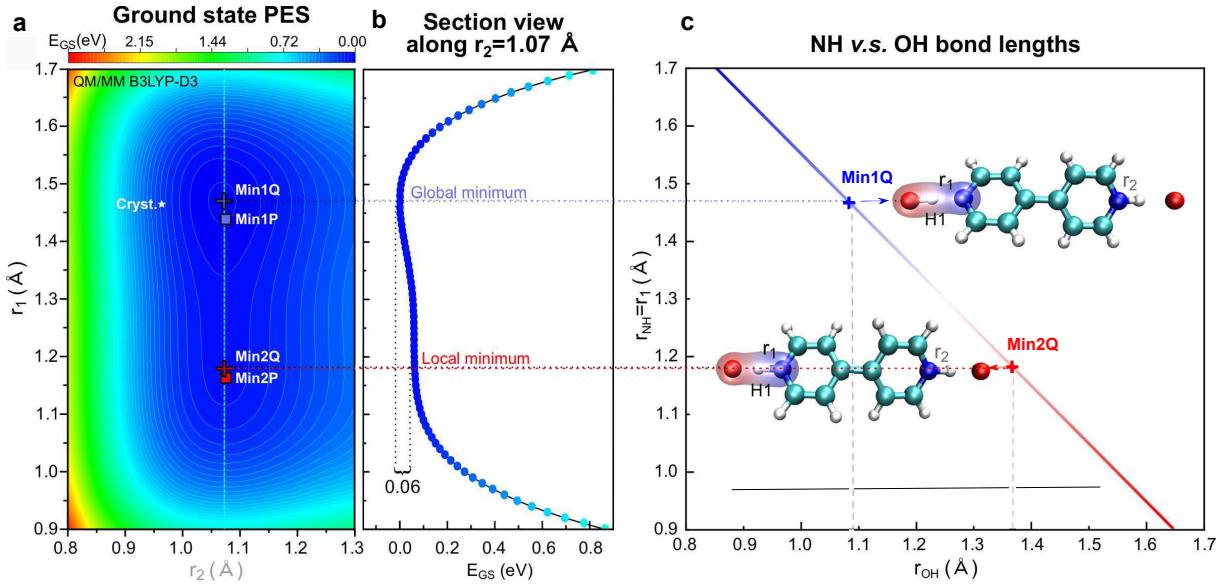

Fig. 3 (a) 2D contour map of the ground state PES computed by the QM/MM method (B3LYP-D3/NPA). "+" denotes the predicted two minima (**Min1Q** and **Min2Q**). Two PBC-optimized structures **Min1P** and **Min2P** (■) and the crystal structure **Cryst.** (∗) are also indicated for comparison. (b) Section view along the line of r_2=1.07 Å in the PES (vertical dashed line in panel a). (c) For each data point in panel b, corresponding N1-H1 distance (r_{NH}=r_1) and O1-H1 distance (r_{OH}) can be read. Inset: structures of **Min1Q** (N–H$^+$···O$^-$) and **Min2Q** (N···H–O) exhibiting two different types of HBs at N1.

Effects of geometrical relaxations

The hydrogen position is challenging to resolve by XRD, prompting us to attempt relaxing the experimental geometry and then simulating XPS spectra based on it. We expected improved results compared to those based on the crystal structure. Utilizing the PBE-D3[?] and PBE[?] functionals, we obtained two minima structures, **Min1P** and **Min2P**, respectively, with periodic boundary conditions (PBCs). It was found that including the dispersion correction (PBE-D3) allowed us to achieve the same protonation state as the crystal structure (Figure 2a). However, deactivating this correction led to the identification of another HB structure (charge-assisted HB, N–H$^+$···O$^-$) at N1, deviating from the experiment (neutral HB, N···H–O). All three structures exhibited the same HB type at N2 (N–H$^+$···O$^-$).

Figure 2b shows the computed spectra for the three structures (**Cryst.**, **Min1P**, and **Min2P**), compared with the experiment.[?]

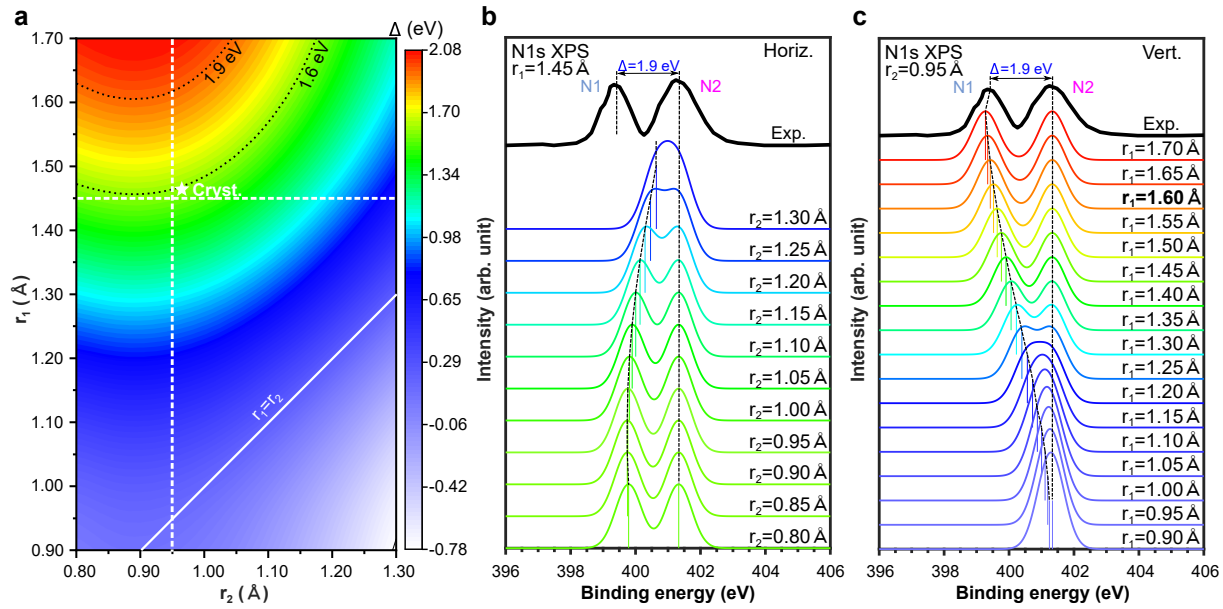

Fig. 4 Dependence of XPS chemical shift Δ on H positions in BSC. (a) 2D contour map of Δ simulated by QM/MM with respect to two distances r_1 (H1-N1) and r_2 (H2-N2) along the H-N lines (the rest atoms were frozen). See structure in Figure 1b. (b-c) Simulated N1s XPS by QM/MM along the two dashed lines in panel a. All theoretical spectra were uniformly shifted by δ (see Tables S5–S6) to better compare with the experiment[?] by aligning the high-energy peak. In panel c, the distance that exhibits optimal agreement with the experiment is highlighted in bold.

The calculation performed at **Min2P** only predicted a single peak (convoluted from two stick BE values with a separation of 0.3 eV). This discrepancy clearly indicates that **Min2P** is an incorrect structure when compared to the experiment. Although the double-peak feature was reproduced at **Min1P**, the calculated chemical shift of 1.1 eV did not improve the agreement with the experiment[?] (deviating by 0.8 eV) compared to the calculation directly at the crystal structure (deviating by 0.4 eV). Our results suggest that locating minima in such organic crystals with localized charges and strong HB networks poses a challenge in quantum chemistry. To relax crystal geometries in PBC calculations, more advanced electronic methods are necessary.[? ?] However, it may come with certain requirements on expensive computational costs or specialized expertise.

Ground-state potential energy surfaces

QM/MM serves as an alternative protocol to PBC calculations, offering greater flexibility in the selection of density functionals. Instead of conducting geometry optimizations, we employed QM/MM to construct the PESs, utilizing the hybrid B3LYP-D3 functional.[? ?] It is crucial to consider that the positions of atoms, particularly H atoms, can be influenced by environmental factors such as temperature and pressure, causing deviations from their equilibrium positions. To address the impact of hydrogen positions and achieve a comprehensive understanding of the energy landscape and transition energies, ground-state PESs were generated, based on which vertical core ionization/excitations were calculated.

In particular, we investigated the effects of hydrogen positions by scanning the two N-H distances for the central residue, N1–H1 (r_1) and N2–H2 (r_2). That is, {r_1, r_2} was taken as a compound reaction coordinate ζ. Figure 3a shows a 2D contour map of the computed PES to r_1 and r_2, predicting two minima at r_1=1.47 (**Min1Q**, the global minimum) and 1.18 Å (**Min2Q**, a local minimum), both at almost the same r_2=1.07 Å . As shown in Figure 3b, **Min1Q** and **Min2Q** correspond to N···H–O and N–H$^+$···O$^-$ types of hydrogen bonds at N1, respectively. The two minima obtained from the PES scan at the QM/MM level align respectively with **Min1P** and **Min2P** from periodic relaxations (Figure 3a). For validation purposes, additional QM/MM PES calculations were also performed by replacing B3LYP with the PW6B95D3 functional[?] for the QM part, and consistent predictions were obtained (Figure S2).

2D map of the XPS chemical shifts

To explore the connection between structure and X-ray spectra along the proton transfer pathway, we conducted simulations of transient XPS and XAS spectra at various snapshots based on the crystal structure with different hydrogen positions. Figure 4 presents a 2D map of the XPS chemical shift (Δ) to r_1 and r_2, based on cluster model 2' (Figure S3b) and NPA charges. This QM model was selected to balance accuracy and efficiency. As shown in Figure 4a, Δ is more sensitive to variations in r_1 than r_2, increasing proportionally as r_1 increases. Conversely, the influence of r_2 on Δ is less pronounced. The 2D map can be divided into two regions based on the values of r_1 and r_2: $r_1 > r_2$ and $r_1 < r_2$. Along the diagonal where $r_1 = r_2$ (solid white line), both nitrogens have similar local chemical environments, resulting in a very small Δ. While most values in this map are positive, negative values are also present (seen in the bottom right corner), indicating a switch in the order of the two binding energies. The calculated value for the crystal structure (Δ=1.6 eV) deviates from the experimental

chemical shift (1.9 eV) by 0.3 eV. The contour map indicates that the experimental Δ corresponds to a broader range of r_1 (1.6–1.7 Å) (dotted contour lines) compared to r_1 =1.461 Å at the crystal structure. This corresponds to a smaller O1–H1 distance (0.854–0.953 Å) compared to 1.091 Å at the crystal structure. In other words, if the O1–H1 distance decreases by approximately 0.2 Å from the XRD crystal structure, it can accurately reproduce the experimental XPS spectrum.

Further, we examined the impact of a single variable, either r_1 or r_2, on Δ. Figure 4 b–c shows the simulated XPS spectra to r_1 (vertical line) or r_2 (horizontal line). As depicted in panel b, varying r_2 from 1.3 to 0.8 Å while keeping r_1 fixed at 1.45 Å leads to an increase in the chemical shift from 0.7 to 1.6 eV. Conversely, Δ monotonically decreases from 2.1 to 0.1 eV as r_1 shifts from 1.7 to 0.9 Å while keeping r_2 fixed at 0.95 Å (panel c). Notably, at $r_1 = 1.60$ and $r_2 = 0.95$ Å, the predicted Δ of 1.9 eV aligns excellently with the experiment. Detailed Δ and δ values are provided in Tables S5–S6.

2D map of the XAS π^*-peak separations

Figure 5 displays the simulated N1s XAS spectra of BSC with varying hydrogen positions. The 2D contour maps of π_1^* and π_2^* energy positions are respectively depicted in Figure 5 a–b, and the separation D between the two peaks in Figure 5c. Increasing r_1 from 0.9 to 1.7 Å results in a red shift of the π_1^* energy by ca. 1.4 eV (from 399.55 to 398.15 eV), while changes in r_2 barely influence the transition energy. For instance, changing r_2 from 0.8 to 1.3 Å based on the crystal structure (along the horizontal dashed line) only shifts the transition energy by about 0.1 eV. Similarly, changing r_1 from 0.9 to 1.7 Å only slightly increases the π_2^* peak by ca. 0.2 eV (Figure 5b). Interestingly, the increase of r_2 leads to a blue shift followed by a red shift of the π_2^* energy (399.60–399.75 eV, 0.80–1.00 Å; 399.75–399.25 eV, 1.00–1.30 Å). This can be explained by the fact that π_1^* is entirely contributed by N1, while π_2^* has a small contribution from N1 in addition to N2 (Figure 1f). Therefore, the change of r_1 has a significant impact on π_1^* and a small impact on π_2^*, whereas the change of r_2 only impacts π_2^*. Consequently, we observed a monotonous increase in D as r_1 increases, and a general trend of initial increase followed by a decrease in D as r_2 increases (Figure 5c). In the range determined by XPS spectral simulation (Figure 4), 1.6–1.7 Å of r_1, D reaches the maximum value of 1.60 eV, which is about 0.2 eV lower than experimental D (1.79 eV). However, the computed D at the crystal structure (r_1=1.461 Å) is 1.08 eV. In comparison, simulations with larger r_1 (1.6–1.7 Å) can better reproduce the experimental XAS spectrum, which is consistent with XPS results.

Figure 5 d–g illustrates the total (panels d and f) and atomic-specific (panels e and g) spectra with a single variable r_1 or r_2. When r_2 increases with r_1 fixed at 1.45 Å (Figure 5d), the total spectrum evolves from two peaks to one peak (D is changed from 1.05 to 1.20 and then to 0.60 eV), due to a slight blue shift followed by a red shift of the N2 peak as well as almost no shift of the N1 peak (Figure 5e). In Figure 5f, an increase in r_1 while keeping r_2=0.95 Å triggers a transition in the total spectrum. Initially, we observe a high-intensity peak paired with a low-intensity peak, which subsequently evolves into a configuration of one dominant peak succeeded by two peaks of equal intensity. Accompanying this spectral evolution, there is a notable increase in the separation D, escalating from 0.1 to 1.60 eV. In Figure 5g, the atom-specific spectra indicate that the N1 peak undergoes a redshift, and the N2 peak hardly shifts with increasing r_1. The overlapping of the high-energy tails of N1 and N2 peaks results in the low-intensity peak in panel f.

Tracking the XAS peak energy to proton transfer N–H$^+$···O$^-$ ↔ N···H–O

Figure 6 depicts the π_1^* and π_2^* absorption energies in the simulated XAS spectra as a function of the N–H distances r_1 and r_2, respectively. As the N–H distances vary from 0.8 to 1.7 Å, the hydrogen bonds transition from N–H$^+$···O$^-$ to N···H–O, causing the photon energy to change by 1.3 eV (398.2–399.5 eV for π_1^*, 398.4–399.7 eV for π_2^*). Both curves exhibit a maximum at $r_{N\text{-}H}$=0.95 Å, displaying a slight increase followed by a rapid decrease.

In experimental transient X-ray spectral studies, it is common that one follows the evolution of a characteristic peak (energy and/or intensity) to study the dynamics, which can then be used to develop kinetic models. Our simulation, based on PES snapshots, offers a continuous view of the characteristic π^* peaks in the proton transfer process, which could be referenced in future experimental transient XAS studies. The similarity in π_1^*–r_1 and π_2^*–r_2 curves further indicates that the two nitrogens are decoupled in the X-ray processes, in line with the locality of core excitations. Additionally, the absorption energy added to the ground state energy gives the PES of the core-excited state (Figure S6).

Discussion

Influences of functionals and protonation

One essential parameter of our DFT/MM protocol is the functional used. To assess its impact on the computed N1s BEs, tests were done in the gas phase. Using BpyH$^+$ and Bpy (Figure S5), four functionals, BP86, M06-2X, B3LYP, and CAM-B3LYP, were selected for validation. Table 1 demonstrates that all functionals produce similar results, with a maximum difference of ca. 0.2 eV for both absolute BEs and chemical shifts. The standard deviation induced by the functional is estimated to be approximately 0.1 eV (half of the maximum difference). The chemical shift between the protonated (N2) and unprotonated (N1) nitrogens in BpyH$^+$, Δ, ranges 4.3–4.5 eV (BP86, 4.3 eV; B3LYP/M06-2X, 4.4 eV; CAM-B3LYP, 4.5 eV). While it is more expensive to conduct such an analysis for the crystal phase, similar accuracy can be approximated due to the locality of core excitations.

The protonation of Bpy to BpyH$^+$ causes a great change in the N1s BE. Even for the unprotonated nitrogen (N1), its BE increases by 3.3 eV from 403.95 to 407.23 eV, taking the BP86 result as an example. The protonated nitrogen experiences a more pronounced blue shift at 411.50 eV. Our analysis in the gas phase indicates that the influence of functionals is relatively weak compared to the strong influence of protonation.

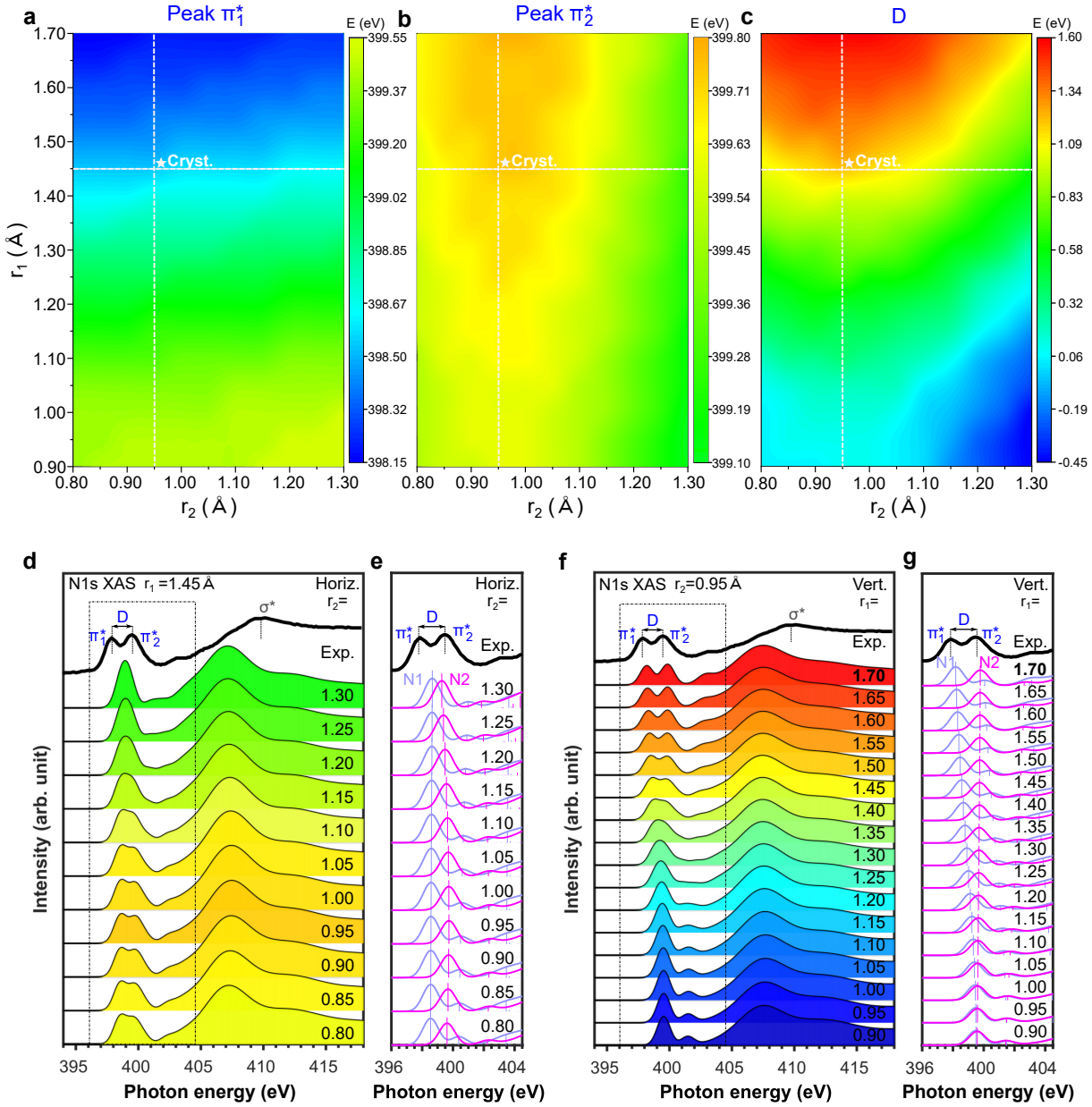

Fig. 5 Simulated N1s XAS of BSC by QM/MM. (a-c) 2D contour map of the (a) π_1^* and (b) π_2^* peaks, and (c) their chemical shift D to distances r_1 (H1-N1) and r_2 (H2-N2). (d-g) Analysis of atom-specific contributions along the (d-e) horizontal and (f-g) vertical dashed lines defined in panels a-c. Total theoretical and experimental[?] spectra are also included for comparison. No *ad hoc* shift was applied. In panels f and g, the distance that exhibits optimal agreement with the experiment is highlighted in bold.

Influence of the crystal environment

A comparison of results in the gas and solid phases (Table 1) reveals the influence of the crystal environment, primarily attributed to the intermolecular hydrogen bonds and the Coulomb interactions. The chemical shift is reduced from 4.27 eV (by BP86) in the gas phase to 1.49 eV in the crystal phase (by BP86/NPA). These results suggest that in the crystal, the complex hydrogen bonding network and Coulomb interactions correlate the two nitrogens, making their local chemical environments less different.

Influence of the ΔKS scheme

We further discuss the accuracy of the ΔKS scheme in producing the absolute BEs and chemical shifts. In the gas phase, the ΔKS method can typically predict the absolute BE with sub-electronvolt[?,?,?,?,?,?] (0.21,[?] 0.3,[?] 0.81,[?], 0.5–1.0[?] eV) accuracy compared to experiments. Calculating core-level BEs for crystals poses additional challenges due to their more complex structures and interactions as compared to gas-phase molecules. For a long time, relative BEs were used for solids and surfaces. Recent developments include methods based on the ΔSCF strategy,[?,?] the quasi-particle GW scheme,[?,?] and their combination.[?] With the cluster-periodic method based on the ΔSCF

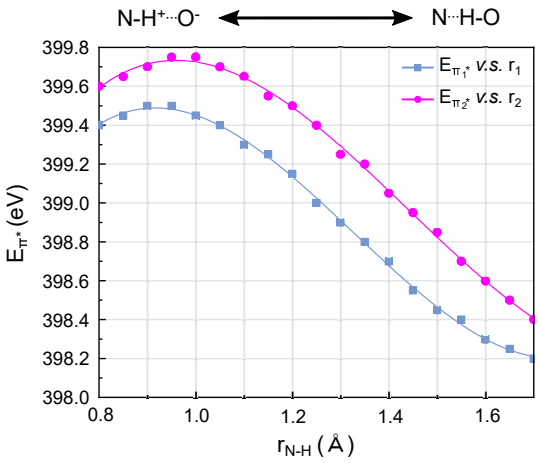

Fig. 6 Tracking the π^* peak energies in response to changes in N-H distances (N–H$^+$ ···O$^-$ ↔ N···H–O). The skyblue line shows the evolution of the π_1^* position (corresponding to the vertical dashed line in Figure 5a or peak N1 in Figure 5g) along r_1 (N1-H1), with r_2 fixed at 0.95 Å. The magenta line depicts the evolution of the π_2^* position (corresponding to the horizontal dashed line in Figure 5b or peak N2 in Figure 5e) along r_2 (N2-H2), with r_1 fixed at 1.45 Å. Both have been extended to a wider distance region.

Table 1 Computed 1s binding energies (in eV) for protonated (N2) and unprotonated (N1) nitrogens of Bpy and BpyH$^+$ in the gas phase by DFT with different functionals and in the BSC crystal by BP86/NPA.

	Bpy	BpyH$^+$		
Functional	N1	N1	N2	Δ[a]
Gas phase				
BP86	403.95	407.23	411.50	4.27
M06-2X	404.00	407.18	411.61	4.43
B3LYP	404.00	407.25	411.62	4.37
CAM-B3LYP	404.15	407.35	411.84	4.49
Crystal phase				
BP86/NPA	–	399.84	401.33	1.49
Expt.[b]	–	399.40	401.33	1.93

[a] Δ ≡ IP(N2) − IP(N1).
[b] Experiment by Stevens et al.[?]

scheme,[?] an accuracy of 0.1–0.2 eV (0.5–0.8 eV) at N1s (C1s) edge was obtained. The GW approximation incorporating the dynamical screening effect gives mean absolute deviations (MADs) of 0.5–0.6 eV for periodic solid systems.[? ?] The combination of ΔSCF and GW gives an improvement for semiconductors while a regression for metals.[?]

The accuracy of relative BE (ΔBE) using the ΔKS approach is comparable or smaller to that of absolute BE. For instance, MADs of 0.21 eV (by TPSS) and 0.81 eV (by PBE) in absolute BE correspond to MADs of 0.25 and 0.24 eV in chemical shifts.[?] With the DFT/NPA method, a deviation of 0.0–0.3 eV (0.2 eV on average) was found for three organic crystals.[?] In this context, a deviation of chemical shifts of 0.4 eV at the XRD structure by DFT/NPA is considered acceptable.

Influence of hydrogen positions

The observed deviation could be attributed to the determination of hydrogen positions, which are sensitive to the surrounding environment and can significantly affect the 1s BEs of the N atom within the hydrogen bond. Crystal structure detection by XRD and X-ray spectra may be performed under different ambient conditions.[? ? ?] To account for the effect of these external perturbations, we phenomenologically moved two protons along the HBs and consequently observed that a reduction of 0.2 Å of O–H distance from the XRD structure can consistently reproduce both XPS and XAS spectra. Interestingly, this adjustment coincided with previous observations[?] in another organic crystal.

Theory: dynamical *versus* static approaches

Ultrafast spectroscopic study of ultrafast chemical reactions follows a research paradigm of "electronic structure→molecular dynamics→signal".[?] The direct solution involves dynamics at various levels (such as ab initio, nondiabatic, quantum wavepacket),[? ? ? ?] which is computationally expensive to reach the statistical average for relatively large systems or long dynamics. This serves as the bottleneck of linking between experiment and simulation. An alternative approach is by using the static PES[? ?] which inherently considers the statistical effect. This procedure is simple, economical, and practical for structurally complex organic crystals with many localized charges. In this work, core excitation/ionization was carried out at snapshots along the ground-state PES, providing valuable insights for more complex ESIPT studies of solids involving multiple valence-excited states.

Experiment: structure dynamics by ultrafast spectroscopy *versus* scattering

Structure dynamics can be investigated by using ultrafast (X-ray, electron, and neutron) scattering and ultrafast X-ray spectroscopy, offering complementary insights into ultrafast chemical reactions and physical processes.[?] Ultrafast X-ray diffraction[? ?] provides a direct view into the 3D structures of transient intermediates. The advancement of XFEL sources has made time-resolved crystallography,[?] down to femtosecond scale, more accessible. However, X-ray diffraction is not effective for studying the dynamics of hydrogen atoms. On the other hand, neutron scattering is suitable for determining hydrogen position, accompanied with a large background caused by incoherent cross-sections. Time-resolved neutron scattering[?] experiment usually has a lower time resolution than with X-rays (the latest study reported nanosecond scale[?]). Ultrafast electron diffraction (UED)[? ?] exhibits stronger interactions compared to X-rays, making it effective in probing gas-phase, thin-film, and surface samples.[?] However, probing condensed samples like liquids presents a challenge due to the limited penetration depth of electrons. In this work, we demonstrated the sensitivity and power of ultrafast X-ray spectroscopy in probing the PT dynamics. Furthermore, the study of crystal phases with rigid structures provides a basis for addressing more complex solution-phase and biological problems. For example, with ultrafast X-ray spectroscopy, a long debate of the phases of over-cooled water was resolved.[? ?] Additionally, ultrafast elec-

tron microscopy (4D UEM)[?] offers a promising alternative avenue for exploring PT dynamics.

Conclusion

To summarize, our study employed QM/MM calculations to investigate the change in N1s XPS/XAS spectra in a complex organic crystal in the proton transfer pathway. The resulting transient XPS/XAS spectra, in relation to the HB distance, confirmed that both spectra are sensitive to the hydrogen position, providing valuable insights into the structure-spectroscopy relation. Our systematic simulation revealed that decreasing the O–H distance at the carboxyl group by ca. 0.2 Å from the XRD crystal structure better reproduced the experimental XPS and XAS spectra consistently. With increasing N-H distance, the energy of the π^* peak in XAS shows a barrier peaked at around 0.95 Å.

The converged relative binding energy of the crystal structure by QM/MM deviated ≤0.4 eV to the experiment. The separation of the two π^* peaks in XAS showed a deviation of ca. 0.3 eV. Furthermore, the simulated spectra on the two optimized geometries and the ground-state PES confirmed that the N1 site was unprotonated and the N2 site was protonated, consistent with the crystal structure. When analyzing the gas-phase molecule (Bpy) and cation ($BpyH^+$) using four types of functionals to assess the accuracy of our protocol, the results indicated that different functionals produced a deviation of approximately 0.2 eV of Δ. Compared to the crystal results, the complex hydrogen bonding network and Coulomb interactions in the crystal eliminated discrepancies between the local environments of both nitrogens. Our findings demonstrate that theoretical XPS and XAS spectra can accurately determine the hydrogen position in organic proton-transfer crystals, and we anticipate applying these computed X-ray spectra to resolve the ultrafast proton transfer dynamics in complex organic crystal materials.

Computational methods

The QM/MM method[?] was utilized to simulate the N1s XPS/XAS spectra of the BSC crystal. A 3×3×3 supercell was chosen as the model for the consequent QM/MM study. Four clusters with increasing sizes (models 1-4; Figure S1) were constructed as the QM parts, and the rest atoms are the MM parts. DFT with the BP86 functional[??] was used for the QM part, and point charges obtained by using the natural population analysis (NPA)[?] were employed for the MM part. Further details can be found elsewhere[?], and validations with other types of point charges are provided in Supplementary Note 2.

Periodic calculations for BSC were performed with the VASP package[?] based on the primitive cell. The PBE functional[?] with and without including the van der Waals (vdW) corrections was employed. When considering the vdW effect, the Becke-Jonson (BJ) damping[?] was evoked for calculating the dispersion correction term within the DFT-D3[?] method, as denoted by PBE-D3(BJ). PBE-D3(BJ) and PBE relaxations lead to two minimum-energy structures **Min1P** and **Min2P**, respectively. Theoretical XPS spectra were uniformly shifted by δ by aligning the high-energy peak to the experiment.[?] XPS spectrum was generated by convoluting stick spectra of IPs with a Gaussian line shape with half-width-at-half-maximum (HWHM) set at 0.47 eV. XAS spectra were generated from stick spectra by Gaussian convolution with varying HWHM values: 0.6 eV below 403 eV, 1.8 eV above 404 eV, and linearly increasing HWHMs in between. No *ad hoc* shift was applied. More details are given in Supplementary Note 1.

Author Contributions

W. H. designed the research. G. G. performed all calculations with the help of other coauthors. G.G., K.E., and W.H. wrote the manuscript. All authors discussed the results.

Notes

The authors declare no competing financial interest.

Acknowledgements

Financial support from the National Natural Science Foundation of China (Grant No. 12274229) is greatly acknowledged.

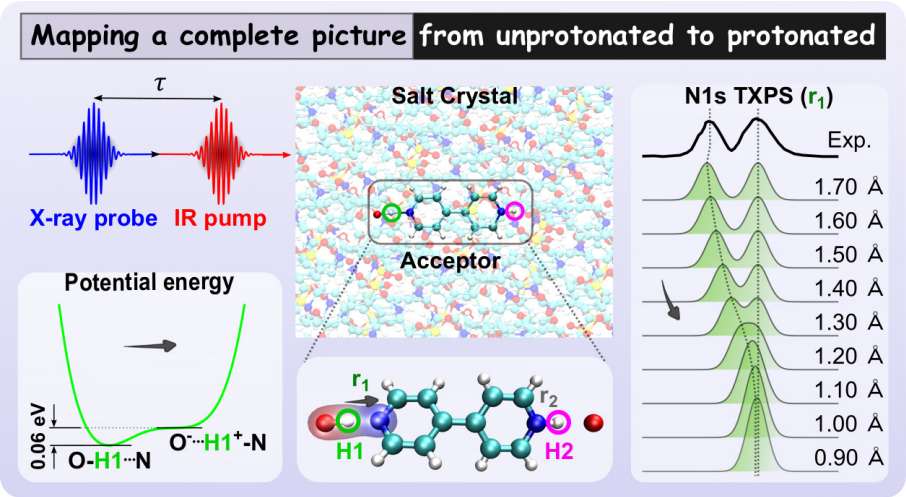

TOC graphics Organic crystal: Proton transfer dynamics between O and N can be mapped in N1s XPS and XAS spectra